

A search for ultrahigh-energy neutrinos associated with astrophysical sources using the third flight of ANITA

C. DEACONU,¹ L. BATTEN,² P. ALLISON,³ O. BANERJEE,³ J. J. BEATTY,³ K. BELOV,⁴ D. Z. BESSON,^{5,6} W. R. BINNS,⁷ V. BUGAEV,⁷ P. CAO,⁸ C. H. CHEN,⁹ P. CHEN,⁹ Y. CHEN,⁹ J. M. CLEM,⁸ A. CONNOLLY,³ L. CREMONESI,¹⁰ B. DAILEY,³ P. F. DOWKONTT,⁷ B. D. FOX,¹¹ J. W. H. GORDON,³ P. W. GORHAM,¹¹ C. HAST,¹² B. HILL,¹¹ S. Y. HSU,⁹ J. J. HUANG,⁹ K. HUGHES,^{1,3} R. HUPE,³ M. H. ISRAEL,⁷ K. M. LIEWER,⁴ T. C. LIU,^{9,13} A. B. LUDWIG,¹ L. MACCHIARULO,¹¹ S. MATSUNO,¹¹ K. MCBRIDE,³ C. MIKI,¹¹ K. MULREY,⁸ J. NAM,⁹ C. NAUDET,⁴ R. J. NICHOL,² A. NOVIKOV,^{5,6} E. OBERLA,¹ S. PROHIRA,^{3,5} R. PRECHELT,¹¹ B. F. RAUCH,⁷ J. RIPA,⁹ J. M. ROBERTS,^{11,14} A. ROMERO-WOLF,⁴ B. ROTTER,¹¹ J. W. RUSSELL,¹¹ D. SALTZBERG,¹⁵ D. SECKEL,⁸ H. SCHOORLEMMER,¹¹ J. SHIAO,⁹ S. STAFFORD,³ J. STOCKHAM,⁵ M. STOCKHAM,⁵ B. STRUTT,¹⁵ M. S. SUTHERLAND,³ G. S. VARNER,¹¹ A. G. VIEREGG,¹ N. WANG,¹⁵ S. H. WANG,⁹ S. A. WISSEL,¹⁶

THE ANITA COLLABORATION

¹Dept. of Physics, Enrico Fermi Inst., Kavli Inst. for Cosmological Physics, Univ. of Chicago, Chicago, IL 60637.

²Dept. of Physics and Astronomy, Univ. College London, London, United Kingdom.

³Dept. of Physics, Center for Cosmology and AstroParticle Physics, The Ohio State Univ., Columbus, OH 43210.

⁴Jet Propulsion Laboratory, California Inst. for Technology, Pasadena, CA 91109.

⁵Dept. of Physics and Astronomy, Univ. of Kansas, Lawrence, KS 66045.

⁶Moscow Engineering Physics Inst., Moscow, Russia.

⁷Dept. of Physics, McDonnell Center for the Space Sciences, Washington Univ. in St. Louis, MO 63130.

⁸Dept. of Physics, Univ. of Delaware, Newark, DE 19716.

⁹Dept. of Physics, Grad. Inst. of Astrophys., Leung Center for Cosmology and Particle Astrophysics, National Taiwan Univ., Taipei, Taiwan.

¹⁰School of Physics and Astronomy, Queen Mary Univ. of London, London, United Kingdom.

¹¹Dept. of Physics and Astronomy, Univ. of Hawaii, Manoa, HI 96822.

¹²SLAC National Accelerator Laboratory, Menlo Park, CA, 94025.

¹³Dept. of Electrophysics, National Chiao Tung Univ., Hsinchu, Taiwan.

¹⁴Center for Astrophysics and Space Sciences, Univ. of California, San Diego, La Jolla, CA 92093.

¹⁵Dept. of Physics and Astronomy, Univ. of California, Los Angeles, Los Angeles, CA 90095.

¹⁶Physics Dept., Astronomy & Astrophysics Dept. Pennsylvania State Univ., University Park, PA 16802

Submitted to ApJ

ABSTRACT

The ANtarctic Impulsive Transient Antenna (ANITA) long-duration balloon experiment is sensitive to interactions of ultra high-energy ($E > 10^{18}$ eV) neutrinos in the Antarctic ice sheet. The third flight of ANITA, lasting 22 days, began in December 2014. We develop a methodology to search for energetic neutrinos spatially and temporally coincident with potential source classes in ANITA data. This methodology is applied to several source classes: the TXS 0506+056 blazar and NGC 1068, the first potential TeV neutrino sources identified by IceCube, flaring high-energy blazars reported by the Fermi All-Sky Variability Analysis, gamma-ray bursts, and supernovae. Among the five source classes, one candidate was identified as associated with SN 2015D, although not at a statistically significant level. We proceed to place upper limits on the source classes. We further comment on two subthreshold events and potential application of this methodology to more sensitive future instruments.

1. INTRODUCTION

The Antarctic Impulsive Transient Antenna (ANITA) experiment (Gorham et al. 2009a) deploys a balloon-borne radio interferometer to search for the impulsive

Askaryan radio emission (Askaryan 1962; Gorham et al. 2007) expected to be produced by the interactions of ultrahigh-energy (UHE) neutrinos ($E > 10^{18}$ eV) interacting in polar ice. ANITA has previously reported constraints on diffuse UHE neutrinos (Gorham et al. 2009b, 2010, 2018a, 2019) as well as neutrinos in time-coincidence with gamma-ray bursts (GRBs) (Vieregg et al. 2011). So far, no candidate events have been observed above background expectations in the Askaryan channel, but the ANITA program sets the most stringent limits on the diffuse UHE flux at energies above $10^{19.5}$ eV.

Cosmogenic UHE neutrinos are expected to be produced in the interactions of the UHE cosmic-rays (UHECR) with the CMB (i.e. the GZK process) (Greisen 1966; Zatsepin & Kuzmin 1966; Kotera et al. 2010). The sources of the UHECR are unknown, and it is also not known if the sources are transient in nature or steady-state. Typical GZK interaction lengths of a few hundred MPc imply cosmogenic neutrinos will retain the source direction over cosmological distances, but it is likely that time association with potential astrophysical transients will be lost due to deflections of UHECR by intergalactic magnetic fields.

Astrophysical neutrinos, believed to be produced directly in astrophysical sources, have been detected at TeV-PeV energies by IceCube (Aartsen et al. 2013). IceCube has identified evidence for some particular astrophysical neutrino sources, including TXS 0506+056 (Aartsen et al. 2018a,b) and NGC 1068 (Aartsen et al. 2020a). Astrophysical neutrinos may also exist at UHE energies, either as a continuation of the same flux that IceCube has detected, or from other sources, such as flat-spectrum radio quasars (FSRQs) (Righi et al. 2020; Rodrigues et al. 2020) or GRBs (Waxman & Bahcall 2000).

Compared to a diffuse UHE neutrino search, a search for UHE neutrinos associated with particular sources can narrow the detection phase space in direction and, for transient objects, in time. This in general allows a reduction in backgrounds and/or an improvement in analysis efficiency, therefore increasing the sensitivity compared to diffuse fluxes.

In this paper, we build on an ANITA-III diffuse search to develop a methodology to search for UHE neutrinos in spatial and time coincidence with astrophysical source classes. We define a source class as a specification of the time-dependent neutrino flux from one or more sources, $\mathbf{F}(E, t) = \sum_{\text{sources}} F_i(E, t)$. This methodology is applied to the ANITA-III flight for five source classes: TXS 0506+056, NGC 1068, blazars flaring in UHE gamma-rays as identified by the Fermi All-sky Variability Anal-

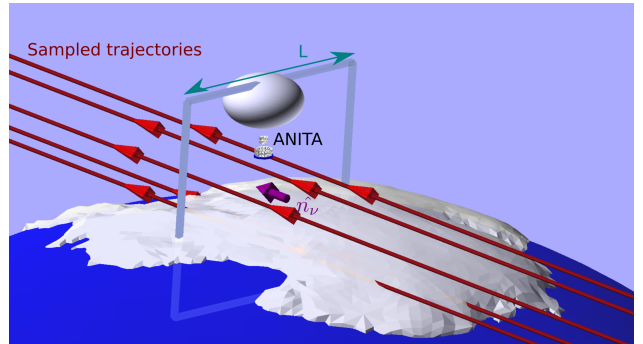


Figure 1. An illustration of the sampling method used for point-source simulation. See text for details.

ysis (FAVA (Abdollahi et al. 2017)), GRBs, and supernovae (SN).

2. SIMULATION

The standard ANITA simulation, `icemc` (Cremonesi et al. 2019), is designed for efficient simulation of a diffuse flux of neutrinos. The default volumetric sampling scheme is very efficient in sampling neutrinos likely to trigger ANITA, but is not appropriate for modeling point sources, as it relies on the “thin target” approximation, converting effective volume to effective area by dividing by the interaction length. As such, a new sampling scheme was developed for this search within `icemc`.

The first step is to choose a payload position/time and neutrino direction. A random time is chosen within the ANITA-III flight which determines the payload position and orientation. The neutrino direction is chosen based on the simulated parameters, for example, a single source, an isotropic flux, or from a collection of time-varying sources.

For a given payload position, \vec{x}_{ANITA} , and neutrino direction \hat{p}_ν , a straightforward way to calculate the effective area for a given neutrino energy, E_ν , is to consider a square with side L , normal to \hat{p}_ν , and throw neutrinos with random trajectories passing through the square (see Fig. 1). Assuming that the square is centered near \vec{x}_{ANITA} (we center it at the ice surface below ANITA) and L is large enough that all neutrinos that trigger ANITA intersect the sampling box, the trigger-level effective area for that configuration is then:

$$A_{\text{eff}}(\hat{p}_\nu, \vec{x}_{\text{ANITA}}, E_\nu) = L^2 \frac{n_{\text{trigger}}}{n_{\text{thrown}}}. \quad (1)$$

A value of $L = 1200$ km is a conservative choice that will miss no events for ANITA-III.

This can readily be generalized to calculating ANITA’s effective area of a point source with sky position Θ by choosing the appropriate \hat{p}_ν at each sam-

pled \vec{x}_{ANITA} , integrating over the flight trajectory by uniformly choosing random times within the flight:

$$A_{\text{eff}}(\Theta, E_{\nu}) = L^2 \frac{n_{\text{trigger}}}{n_{\text{thrown}}}. \quad (2)$$

The remaining difficulty is efficiently calculating n_{trigger} . The naive forward calculation, which involves propagating a neutrino through the Earth until it interacts or exits and checking if ANITA triggers for interacting neutrinos, is computationally wasteful. Instead, the following scheme is used:

1. Check if the neutrino trajectory intersects an ellipsoid defined by the geodesic reference ellipsoid plus 5 km (the highest altitude in Antarctica is 4,892 m). If not, there is no chance of detection, so move on.
2. Find the intersection points of the neutrino with the Antarctic ice volume (as defined by BEDMAP2 (Fretwell et al. 2013)). A step size of 50 m is used in order to detect intersections with ice at least that small. If no intersection with ice is detected, then we have no chance of detecting this neutrino, so move on.
3. In general, there may be multiple intersections with the ice. For each intersecting segment, we calculate a weight, w_s , that is the product of the probability of the neutrino interacting within ice segment and the probability that the neutrino did not interact in the Earth prior to reaching the segment.
4. We choose one intersecting segment at random, and pick an interaction point within that segment with an exponential distribution. We correspondingly multiply w_s by the number of intersecting segments to compensate.
5. We then proceed with the rest of the simulation as usual (e.g. pick interaction type from differential cross-section, sample inelasticity, etc.) and evaluate if ANITA triggers on the radio emission.
6. We now define n_{trigger} as the sum of w_s for events that trigger.

This method can also be used to simulate a diffuse flux by choosing the source direction at random in each trial, effectively performing a Monte Carlo integral over $d\Omega$. By doing so, we can compare to the traditional **icemc** sampling method and find that the diffuse effective areas agree for ANITA-III at the 20% level, which we consider an acceptable level of agreement. The time-averaged

point-source UHE neutrino effective area as a function of declination and energy over the ANITA-III flight is shown in Fig. 2.

Finally, and crucially, this method may easily be adapted to simulate ANITA’s response to a source class. We integrate over the flight trajectory by sampling times during the flight. At each time, we draw from the sources active at the time with probability proportional to its relative flux compared to all other active sources and apply a time weight $w_t = \mathbf{F}(E, t) / \int_{t_0}^{t_1} \mathbf{F}(E, t) dt$.

3. SOURCE SEARCH METHODOLOGY

We will adapt Analysis B from the ANITA-III diffuse search, which is described in detail in the appendices of Gorham et al. (2018a). A brief review is provided here.

3.1. Review of diffuse ANITA analysis

Whenever ANITA triggers, an event is formed from 96 100-ns-long waveforms digitized from 48 dual-polarization antennas with known relative positions and time delays. These waveforms are filtered to remove narrow-band contamination, then an interferometric map is generated for each polarization, where the mean cross-correlation between antennas is plotted as a function of elevation and azimuth in payload-centric coordinates. Directions corresponding to the peaks of these maps are considered hypotheses and coherently-summed waveforms are created in those directions, from which various observables are computed. Analysis B applies three sets of cuts to select diffuse neutrino and air shower candidates:

1. Quality Cuts (\mathcal{Q}), to remove digitizer glitches, radio interference from the payload itself, and other problematic events.
2. A Fisher discriminant, (\mathcal{F}), selecting for neutrino-like events. This discriminant is constructed using a variety of observables about an event’s waveforms (e.g. cross-correlation, signal size, impulsivity, linear polarization) and is trained on a sample of thermal events and simulation, to select impulsive broadband events.
3. A spatial isolation parameter, \mathcal{O} , based on projecting events to the continent, to remove likely anthropogenic events. This parameter is equal to the overlap integral of each event’s pointing resolution projected onto the continent with that of other events. Only events with sufficiently high \mathcal{F} are included in this integral, with a soft turn-on (so that events less likely to be neutrino-like are

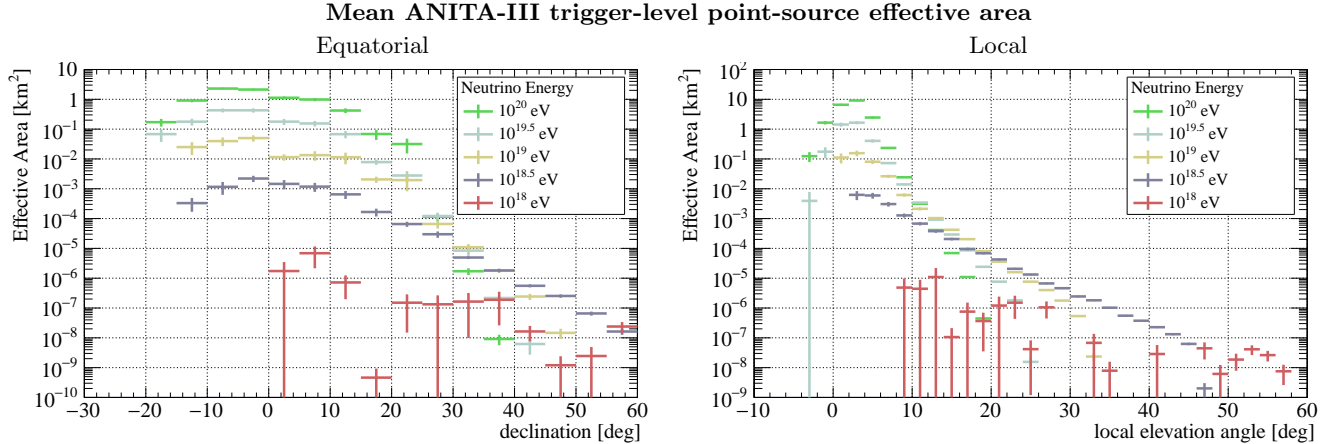


Figure 2. The point-source effective area as a function of declination (left) or local elevation angle (right) averaged over the ANITA-III flight at several energies. Local elevation angle is measured downward from payload horizontal. Because ANITA moves slowly compared to the diurnal cycle, the flight-averaged acceptance is nearly constant with α . The total flight time is 22 days. The point-source simulation results here cannot be directly compared to the diffuse sensitivities quoted elsewhere by ANITA as those are typically geometric averages of multiple independent codes.

given a smaller weight). As \mathcal{O} quickly becomes very small for events that are far apart, it is convenient to set cuts on $-\log_{10} \mathcal{O}$ instead of \mathcal{O} directly.

Events passing that are predominantly vertically-polarized are considered neutrino candidates. \mathcal{Q} was optimized to reduce the number of poor-quality events to a negligible level and then \mathcal{F} and \mathcal{O} each had cut values optimized for sensitivity to a diffuse flux. The primary contribution to the background estimate is anthropogenic, with negligible background from thermal noise, glitches and payload-generated radio interference.

3.2. \mathcal{D} , the source class distance

We now develop a methodology to optimize the search for sensitivity to a given source class rather than a diffuse flux. For expedience, we will keep the definitions of \mathcal{Q} , \mathcal{O} and \mathcal{F} the same, but introduce a new “source distance” parameter, \mathcal{D} , specialized for a given source class. We will then optimize cut values for \mathcal{F} , \mathcal{O} and \mathcal{D} to maximize search sensitivity.

Interferometric event reconstruction produces an estimated direction of the radio emission (ϕ_{RF} , θ_{RF}) in payload coordinates. Since the orientation, time and position of the payload at each event is known, this can be projected into equatorial coordinates, right ascension (α) and declination (δ). Using simulation, these sky distributions of $(\alpha_{RF}, \delta_{RF})$ may be estimated for a neutrino flux.

While this simple method could be used as the basis of a source distance cut, due to the opening angle of the in-ice Cerenkov cone, these distributions are not compact (see Fig. 3, left), which reduces the ability to

efficiently reject background. One way to reduce this dispersion is to estimate the neutrino direction. Because the Askaryan emission is radially-polarized, the observed polarization state of the radio emission from neutrino is related to the neutrino direction. However, this is complicated by instrumental and radio propagation effects and convolved with earth attenuation. The spectrum of the event additionally gives some information about how off-cone the observation is.

For a putative ANITA neutrino candidate, the most robust (albeit model-dependent) way of estimating the neutrino direction is to simulate neutrinos from different directions with the payload fixed at the observation location and then determine which neutrino directions are most compatible with the observed RF direction, polarization, and signal spectrum. However, while doable for an interesting candidate, it is computationally infeasible to use this procedure in a search. Moreover, the primary purpose here is not to reconstruct the most likely neutrino direction, but instead to improve background rejection by constructing a more compact observable. Systematic biases in the direction are not problematic as long as they are present in both data and simulation.

To this end, a large set of isotropic neutrinos were simulated at various energies and run through the same reconstruction framework as data. TMVA (Hoecker et al. 2007) was used to regress a polynomial for $\Delta\phi = \phi_\nu - \phi_{RF}$ and $\Delta\theta = \theta_\nu - \theta_{RF}$ as a function of a number of observables, including the observed coherent waveform polarization state, spectral parameters, signal size, and θ_{RF} . By applying this regression to each event, we can compute an estimator for $\Delta\phi$ and $\Delta\theta$ and therefore the neutrino direction. With knowledge of the payload position and orientation, this can then be projected to our

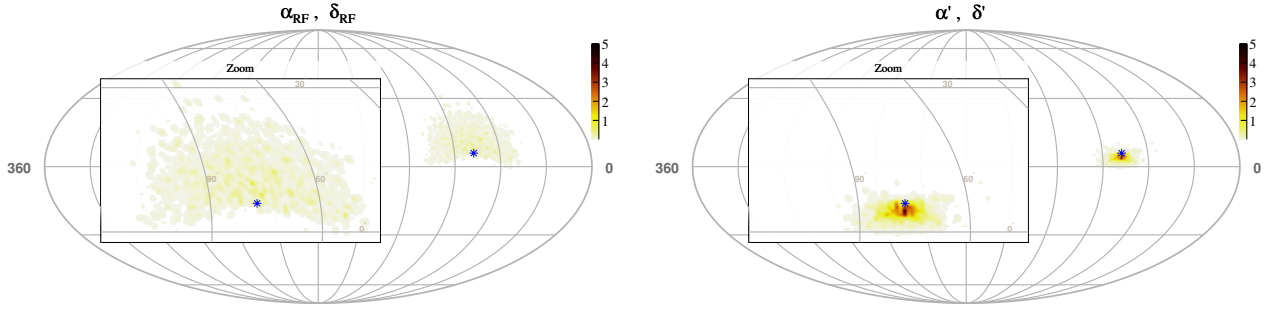


Figure 3. The distribution in equatorial coordinates of the apparent RF direction (left) for simulated neutrinos from TXS 0506+056, and the reconstructed neutrino direction (right) using the approximate reconstruction method described in the text. The more compact distribution allows for improved background discrimination. The color axis depicts the percentage of spatial distribution within each angular bin; bins contributing less than 0.01 percent are not shown for clarity.

equatorial coordinate estimators (α', δ') . We can test the improved compactness of the estimator by applying the reconstruction to Monte Carlo truth, as shown in Fig. 3, right. We find an effective dispersion for the estimator of several degrees in α' and a degree in δ' .

In order to define a source distance parameter in as generic a way as possible, without any assumptions about the shape or modality of the distribution, we use a data-driven histogramming approach. We simulate neutrinos from a source class, process the simulated events, and run the estimator regression to generate a three-dimensional *exposure histogram* with axes of reconstructed α' , δ' , and event time. For a steady source class, the time axis is extraneous and may be ignored. In the case of discrete source turn-on and turn-off times, it is convenient to choose the time bins to align with transitions. This exposure histogram is then converted to an *exposure percentile histogram*, where each bin's value is computed as fraction of the total exposure with differential exposure greater than the differential exposure of

the bin (e.g. Fig. 4). This results in a histogram where the bins with the highest exposure to the source class have values close to 0 and bins with poor or no exposure have a values close to 1. We finally define \mathcal{D} for an event as the value of this exposure percentile histogram for its α' , δ' and event time. This definition has the convenient property that setting the cut on \mathcal{D} to a value $d \in [0, 1]$ roughly selects the highest exposure density and has an efficiency to events from that source class of approximately d .

One technical aspect of \mathcal{D} was deferred until now. Because it is very time-consuming to generate enough simulated events to smoothly fill this exposure histogram at fine resolution, we start with a relatively coarsely binned α' and δ' axes and then use a kernel density estimator in each time slice to create a smoother, more finely-binned histogram. The kernel density estimator scale parameters are tuned so that the distribution of \mathcal{D} for members of the source class is roughly uniform. Small deviations from uniformity are of little concern as long as there is sufficient dynamic range in efficiency versus \mathcal{D} to effectively scan the parameter. To reduce bias, disjoint sets of simulated data are used to create the estimator and for cut optimization, described next.

3.3. Cut Optimization

For each source class, we seek to set optimal cuts in a blind way on the \mathcal{F} (the signal-likeness parameter), \mathcal{O} (the spatial isolation parameter) and \mathcal{D} (the source class distance parameter). We scan in these parameters to optimize expected sensitivity, using:

$$\text{sens.} \propto \left\langle \frac{\text{FC}_{90}(\text{Pois}(\mu_{\text{BG}}), \mu_{\text{BG}})}{\epsilon} \right\rangle, \quad (3)$$

where μ_{BG} is the background estimate for a given set of cuts, ϵ is the expected analysis efficiency for a given set of cuts (the fraction of events that trigger ANITA that also pass analysis cuts), Pois is the Poisson distribution and $\text{FC}_{90}(\text{sig}, \text{bg})$ is the 90% Feldman-Cousins upper

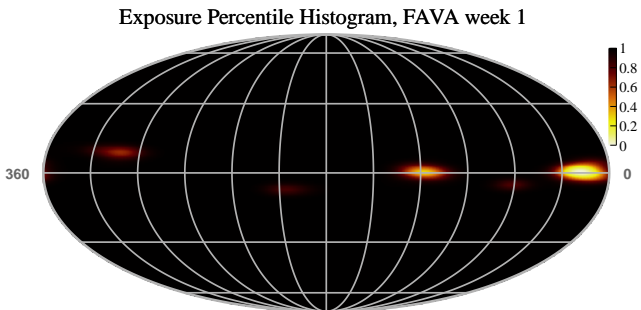


Figure 4. An example time slice of an *exposure percentile histogram*, in this case for the first week of FAVA-detected flaring blazars. The value at each point (α', δ', t) is set to the fraction of the total exposure with differential exposure higher than the differential exposure at the point, so that lower values represent regions of greater exposure. A cut in \mathcal{D} defines the region in (α', δ', t) with value smaller than the cut value, preferentially selecting regions with the greatest exposure density.

limit factor (Feldman & Cousins 1998) for a given number of signal events and background events. The mean is taken here because both μ_{bg} and ϵ have uncertainties, which are integrated over using the semi-Bayesian Cousins-Highland method (Cousins & Highland 1992).

The estimate for analysis efficiency for a given set of cuts may readily be estimated from simulation by simply applying the same cuts to simulated data. A Gaussian systematic error of 10% on the analysis efficiency is assumed, as used in the diffuse analysis.

To estimate the background as a function of cut values, we use a data-driven on-off (Li & Ma 1983) approach based on time shuffling. For each event passing a trial \mathcal{F} and \mathcal{O} , we shift the event time by a random offset between 1.5 hours and 22.5 hours (in either direction) 100 times. These bounds are set so that a significantly different right ascension is guaranteed while preserving some time locality. For each resampling time, we count how often the cut on \mathcal{D} is passed in this off-time sideband (which is at least seven times larger in phase space than the “on-time” region). The posterior on the background estimate is then conservatively taken to be the Poisson posterior using a uniform prior for a sideband eight times larger:

$$p(\mu_{BG}) = \Gamma(7N_{pass}/100 + 1, 1/7). \quad (4)$$

This method is somewhat limited by the statistics of the sideband. As soon as the cuts are so stringent that N_{pass} becomes zero, the background estimate will always be the same ($0.10^{+0.16}_{-0.07}$), no matter how much more the cuts are tightened. Consideration of the efficiency in the sensitivity will typically shift the optimization to the boundary, somewhat alleviating this problem. An alternative would require imposing a background model, which is difficult for the time-varying anthropogenic backgrounds faced by ANITA.

Using this methodology, we can perform a three-dimensional scan over reasonable parameters of \mathcal{F} , $-\log_{10} \mathcal{O}$ and \mathcal{D} to choose cuts that optimize our sensitivity metric for any particular source class. Finally, to avoid selecting air shower events, we only select events that are more impulsive in vertical polarization (VPol) than horizontal polarization (HPol).

4. SOURCES CONSIDERED

Having developed an appropriate methodology, we now turn our attention to potentially interesting sources for ANITA-III. Sources of the same type are pooled together into a single source class in order to reduce the global trials factor. This requires some model dependence in choosing the analysis cuts, but once cuts are chosen, model-independent limits may be placed on

each source within the class. These limits may not be optimal for any given model other than the one used to set cuts, but we make an attempt to adopt a “least-common denominator” set of cuts to minimize the model-dependence.

Each search is optimized and performed independently, but the significance of any particular search’s result must be interpreted in the context of the number of searches performed. We considered optimizing for a global 90% significance (which is roughly equivalent to setting a higher optimized significance in each search, if they are weighted equally), but found that this did not strongly affect where the optimized cuts are placed and we did not want to restrict the possibility of any additional future searches. It is also possible for a given event to be considered a candidate by multiple searches. The considered objects are tabulated in Table 1 and the result of each optimization is shown in Table 2.

4.1. TXS 0506+056

The TXS 0506+056 blazar has been identified by IceCube as a potential source of astrophysical neutrinos. This association is due to a gamma-ray flare in spatial and temporal coincidence with a September 22, 2017 likely astrophysical neutrino candidate that triggered a multi-messenger alert (Aartsen et al. 2018a). Afterwards, archival data suggested an excess of neutrinos from the direction of TXS 0506+056 in a several-month window around December 2014 (Aartsen et al. 2018b), albeit without any gamma-ray activity in the blazar. The ANITA-III flight coincided temporally with this earlier neutrino “burst” and TXS 0506+056, at a declination of 5.6 degrees, is within ANITA-III’s sensitive field-of-view, motivating a dedicated search.

IceCube has measured a spectral index for the neutrino burst of $\gamma = 2.1 \pm 0.2$. To optimize cuts for the ANITA-III search, we simulate neutrinos from the direction of TXS 0506+056 with $\gamma = 2$, which is compatible with the IceCube measurement and somewhat preferred theoretically. The optimization results in an estimated analysis efficiency to an E^{-2} flux of 91.7% with a background estimate of $0.10^{+0.16}_{-0.07}$, which is the minimal background estimate calculable with the method employed (i.e. zero passing sideband events).

4.2. NGC 1068

IceCube has identified NGC 1068 as a potential neutrino point source (Aartsen et al. 2020a) at the 2.9σ level. IceCube does not report any temporal information for NGC 1068, and the best-fit spectral index (3.2) from IceCube would make detection by ANITA-III unlikely. However, as it is one of two just objects within

Objects Considered			
Object	Search	Coordinates	Times Considered (UTC)
TXS 0506+056	TXS 0506+056	$\alpha = 77.4^\circ, \delta = 5.7^\circ$	Full Flight
NGC 1068	NGC 1068	$\alpha = 40.66^\circ, \delta = -0.0^\circ$	Full Flight
3C 454.3	Flaring Blazar	$\alpha = 344^\circ, \delta = 16.1^\circ$	2014-12-15-15:43:38Z + 1 week
4C +01.02	Flaring Blazar	$\alpha = 17^\circ, \delta = 1.6^\circ$	2014-12-15-15:43:38Z + 4 weeks
* B3 1343+451	Flaring Blazar	$\alpha = 206^\circ, \delta = 44.8^\circ$	2015-01-05-15:43:38Z + 1 weeks
CTA 102	Flaring Blazar	$\alpha = 331^\circ, \delta = 11.7^\circ$	2014-12-22-15:43:38Z + 3 weeks
MG1 J221916+1806	Flaring Blazar	$\alpha = 335^\circ, \delta = 18.0^\circ$	2014-12-15-15:43:38Z + 2 weeks
* PKS 0402-362	Flaring Blazar	$\alpha = 61^\circ, \delta = -36.0^\circ$	2014-12-15-15:43:38Z + 4 weeks
PKS 0502+049	Flaring Blazar	$\alpha = 76^\circ, \delta = 5.0^\circ$	2014-12-22-15:43:38Z + 3 weeks
PKS 0736+01	Flaring Blazar	$\alpha = 115^\circ, \delta = 1.5^\circ$	2014-12-15-15:43:38Z + 2 weeks
PKS 1441+25	Flaring Blazar	$\alpha = 221^\circ, \delta = 25.0^\circ$	2014-12-15-15:43:38Z + 4 weeks
PKS 1717+177	Flaring Blazar	$\alpha = 260^\circ, \delta = 17.7^\circ$	2014-12-22-15:43:38Z + 2 weeks
* PKS 1830-211	Flaring Blazar	$\alpha = 278^\circ, \delta = -21.1^\circ$	2015-01-05-15:43:38Z + 1 weeks
PKS 2032+1075	Flaring Blazar	$\alpha = 309^\circ, \delta = 10.9^\circ$	2014-12-15-15:43:38Z + 1 weeks
* PKS 2052-47	Flaring Blazar	$\alpha = 314^\circ, \delta = -47.3^\circ$	2014-12-22-15:43:38Z + 2 weeks
* PKS 2142-75	Flaring Blazar	$\alpha = 327^\circ, \delta = -75.7^\circ$	2014-12-15-15:43:38Z + 1 weeks
PKS B1319-093	Flaring Blazar	$\alpha = 200^\circ, \delta = -9.3^\circ$	2014-12-15-15:43:38Z + 1 weeks
* PMN J2141-6411	Flaring Blazar	$\alpha = 325^\circ, \delta = -64.2^\circ$	2014-12-29-15:43:38Z + 1 weeks
RGB J2243+203	Flaring Blazar	$\alpha = 341^\circ, \delta = 20.3^\circ$	2014-12-15-15:43:38Z + 2 weeks
* S4 +1144+40	Flaring Blazar	$\alpha = 177^\circ, \delta = 40^\circ$	2014-12-22-15:43:38Z + 1 weeks
* S5 +1217+71	Flaring Blazar	$\alpha = 185^\circ, \delta = 71.1^\circ$	2014-12-15-15:43:38Z + 2 weeks
TXS +1100+122	Flaring Blazar	$\alpha = 166^\circ, \delta = 12.0^\circ$	2014-12-29-15:43:38Z + 2 weeks
GRB 141221A	GRB	$\alpha = 198.3^\circ, \delta = 8.2^\circ$	2014-12-21-08:07:02Z $^{+1\text{day}}_{-5\text{min}}$
* GRB 141223240	GRB	$\alpha = 147.4^\circ, \delta = -20.7^\circ$	2014-12-23-05:45:34Z $^{+1\text{day}}_{-5\text{min}}$
GRB 141226880	GRB	$\alpha = 163.9^\circ, \delta = 28.4^\circ$	2014-12-26-21:07:24Z $^{+1\text{day}}_{-5\text{min}}$
GRB 141229911	GRB	$\alpha = 170.1^\circ, \delta = 23.1^\circ$	2014-12-29-21:51:39Z $^{+1\text{day}}_{-5\text{min}}$
* GRB 141229A	GRB	$\alpha = 72.4^\circ, \delta = -19.2^\circ$	2014-12-29-11:48:59 $^{+1\text{day}}_{-5\text{min}}$
GRB 141230834	GRB	$\alpha = 181.5^\circ, \delta = 11.6^\circ$	2014-12-30-20:00:25Z $^{+1\text{day}}_{-5\text{min}}$
GRB 141230A	GRB	$\alpha = 57.0^\circ, \delta = 1.6^\circ$	2014-12-30-03:24:22Z $^{+1\text{day}}_{-5\text{min}}$
GRB 150101B	GRB	$\alpha = 188.0^\circ, \delta = -10.9^\circ$	2015-01-01-15:23:00Z $^{+1\text{day}}_{-5\text{min}}$
GRB 150105A	GRB	$\alpha = 124.3^\circ, \delta = -14.8^\circ$	2015-01-05-06:10:00Z $^{+1\text{day}}_{-5\text{min}}$
GRB 150106921	GRB	$\alpha = 40.8^\circ, \delta = 0.3^\circ$	2015-01-06-22:05:53 $^{+1\text{day}}_{-5\text{min}}$
* SN 2014dz	SN	$\alpha = 52.1^\circ, \delta = 38.0^\circ$	2014-12-10-00:00:00Z + 2 weeks
SN 2014dy	SN	$\alpha = 42.2^\circ, \delta = -0.8^\circ$	2014-12-10-00:00:00Z + 2 weeks
* SN 2015A	SN	$\alpha = 145.3^\circ, \delta = 35.9^\circ$	2015-01-02-00:00:00Z + 2 weeks
SN 2015B	SN	$\alpha = 193.6^\circ, \delta = -12.6^\circ$	2014-12-21-00:00:00Z + 2 weeks
SN 2015D	SN	$\alpha = 198.2^\circ, \delta = 12.6^\circ$	2015-01-06-00:00:00Z + 2 weeks
SN 2015E	SN	$\alpha = 48.4^\circ, \delta = 0.3^\circ$	2014-12-31-00:00:00Z + 2 weeks
SN 2015W	SN	$\alpha = 104.4^\circ, \delta = 13.6^\circ$	2015-01-02-00:00:00Z + 2 weeks

Table 1. All objects considered in this search, along with coordinates and times the source is assumed to be turned on. ANITA-III launched on Dec. 18, 2014 and was terminated Jan 9, 2015. Objects with asterisks were included in the search but resulted in no passing simulated events. The times for the flaring blazar search are one-week time scales based on the Fermi telescope's elapsed mission time, hence the offset of 15:43:38 for each start time.

Optimized cut values

Search	\mathcal{F}	$-\log_{10} \mathcal{O}$	\mathcal{D}	exp. ϵ	exp. backg.
TXS 0506+056	1.7	0.9	0.99	91.7%	$0.10^{+0.16}_{-0.07}$
NGC 1068	2.8	0.5	0.99	93.9%	$0.10^{+0.16}_{-0.07}$
FAVA blazars	2.3	0.9	0.96	82.2%	$0.30^{+0.25}_{-0.16}$
GRBs	1.7	0.1	0.96	92.7%	$0.10^{+0.16}_{-0.07}$
SN	2.3	0.9	0.99	93.0%	$0.23^{+0.22}_{-0.13}$

Table 2. The optimized efficiency and background for each search performed for ANITA-III. The quoted efficiency is calculated for the model used to optimize the cuts and has an estimated uncertainty of order 10%. The background is model-independent. The 16%, 50% and 84% quantiles of the posterior distribution are used to determine the central value and errors quoted.

ANITA’s field of view that has been identified as a potential high-energy neutrino source at this significance level, a search is justified.

As the best-fit spectral index of $\gamma = 3.2$ is not amenable for ANITA’s sensitivity, and moreover, there is no guarantee that any particular source would have consistent spectral index over many orders of magnitude, so we set cuts by simulating neutrinos from NGC 1068 with $\gamma = 2$, resulting in an estimated analysis efficiency of 93.9% and a background of $0.10^{+0.16}_{-0.07}$ (the minimal allowed).

4.3. Flaring Blazars

Motivated in part by the apparent TXS 0506+056 flare coincidence, we consider blazars within the field of view of ANITA-III that are flaring in GeV gamma-rays as potential UHE sources. We use data from the Fermi Large Aperture Telescope’s All-sky Variability Analysis (FAVA) (Abdollahi et al. 2017) to select flaring objects labeled as blazars by 3FGL (Acero et al. 2015) during the ANITA-III flight. FAVA reports on a one-week cadence, during which we assume the flux is constant.

To set cuts, we weight neutrino flux from each blazar equally. While weighting by gamma-ray flux or luminosity distance are also reasonable, equal weighting is the least model-dependent, making it less likely to miss any interesting source. As before, we assume $\gamma = 2$. The result of the optimization is an analysis efficiency estimate of 82.8% and an estimated background of $0.30^{+0.25}_{-0.16}$.

4.4. GRBs

GRBs, the brightest known transient events in the universe, have long been considered a potential source of UHE neutrinos (Waxman & Bahcall 2000). ANITA is

most likely most sensitive to the GRB afterglow neutrino flux, which is expected to have $\gamma = 3/2$ up to some maximum energy (model-dependent, but typically order EeV).

We select GRBs from the IceCube GRBWeb catalog (Coppin 2020), which itself collects data from several sources (Lien et al. 2016; von Kienlin et al. 2020). To optimize cuts, we chose to adopt a $\gamma = 3/2$ spectrum, typical of afterglow models, up to 10 EeV for each GRB, starting five minutes before the GRB and extending 24 hours after. While most models would not predict neutrinos up to 10 EeV for most GRBs, this choice is inclusive and will avoid missing any potential signals. This time window would also tend to accept prompt and precursor neutrinos. The period of 24 hours is chosen as a compromise between too short a window, which might reject some of the most energetic afterglow neutrinos and too long a window, which increases the possibility of chance coincidence. The normalization of each source’s flux was assumed to be proportional to the GRB fluence, using a reasonable minimum value if it is not known. Only GRBs with a declination within 30 degrees of the equator are considered. The cut optimization indicates an estimated analysis efficiency of 92.7% and a minimal background estimate of $0.10^{+0.16}_{-0.07}$.

4.5. Supernovae

Supernovae (SN) are not as popular a source for UHE neutrinos as the previous classes, but have been predicted to produce UHE particles in some models (Wang et al. 2007; Biehl et al. 2018; Alves Batista & Silk 2017) and their transient nature makes them amenable to a source search. Furthermore, the upward-air shower candidate in ANITA-III was spatially coincident with Supernova 2014dz (Gorham et al. 2018b), which likely occurred only several days before, further motivating a search in the Askaryan channel.

Due to a lack of clear model guidance for setting cuts, we select $\gamma = 2$ and a two-week period after the estimated explosion date of the supernova, which is generally computing using spectral properties of the light curve at discovery. We select SN from the CBAT catalog (CBAT 2015) and do not distinguish between supernova types. Optimization of cuts results in an estimated analysis efficiency of 93.0% on a background of $0.22^{+0.22}_{-0.13}$.

5. RESULTS AND DISCUSSION

After applying the optimized cuts to each search using the procedure described above, all searches were null except for the SN search, which identified event 83134914 (Fig. 5, left) as potentially associated with SN 2015D ($\mathcal{D} = 0.67$). This is consistent with the background es-

timate for the search ($p = 0.21$), even before accounting for the number of searches performed.

Due to a bookkeeping error in background estimation, initially a looser set of optimized cuts were computed and erroneously applied, which resulted in two additional passing events, 21318591 and 58125945 (Fig. 5 center and right) that did not pass the final, corrected cuts. While these are not considered part of the result, we will comment briefly on them. All three events are summarized in Table 3.

5.1. Candidate Event 83134914

The sole candidate event this search, event 83134914, was previously identified in the ANITA-III diffuse search (Gorham et al. 2018a) as being neutrino-like and extremely isolated. In this search, it was found to be potentially associated with SN 2015D (Jin et al. 2015), which was discovered approximately 10 days after this event and believed to be around two weeks old at the time of discovery.

We note that the estimated position for this event in this search ($\alpha' = 206^\circ$, $\delta' = 13.9^\circ$) differs substantially from what was reported in the diffuse search ($\alpha = 171 \pm 5^\circ$, $\delta = 16.3 \pm 1^\circ$), which would have failed the association cut here. The previous estimate was performed by dedicated simulations with the payload at that position, rather than the approximate method used in this paper. However, the handling of polarization in the simulation software has also been improved since the previous estimate was made, adding another potential source of discrepancy (the original errors did not include any systematic errors on the simulation). We further note that the procedure in this search is not designed to provide a precise localization, but rather to reduce the search space for associations between data and simulated events from each relevant source class. For the purpose of this search, the event is associated even if the localization differs from the previous estimate.

This event points to isolated deep ice, very far from any known anthropogenic activity and would have passed a much more stringent isolation cut. If, hypothetically, the selection cuts were set to barely accommodate this event, the background estimate for the supernova search would be the minimal possible with the method used ($0.10^{+0.16}_{-0.07}$), which would modify the pre-trial significance of this event to $p = 0.13$. This is not enough to be interesting by itself, but is perhaps more interesting in combination with the potential association of the apparently upward air-shower in ANITA-III with an SN, which had $p = 0.0017 - 0.023$, depending on the prior used for the time dependence (Gorham et al. 2018b, Supplemental Material).

To get a feeling for the false association rate, should 83134914 be an anthropogenic event, we consider the sideband of VPol-identified events with $\mathcal{F} \in [1, 2]$, $-\log_{10} \mathcal{O} \in [-1, 1]$. Of these 173 sideband events, 4 (2.3%) would have passed the SN association cut value and just one event has an association as good as the candidate. 22 events (12.7%) in this sideband pass the association cut for any of the five source classes.

It is possible that 3134914 is a UHE neutrino event and not some anthropogenic background, but is associated with a SN direction by chance. By simulating a diffuse cosmogenic neutrino flux we find 10% of simulated diffuse neutrinos would be considered SN-associated in this search and 24% would be considered associated with any of the source classes at each search’s cut level.

A subthreshold search in the direction of SN 2015D down to $\mathcal{F} = 0$ and $-\log_{10} \mathcal{O} = 0$ was performed, yielding one additional event. This event was isolated but was only marginally-associated with SN2014D and upon further inspection, is potentially residual radio interference from satellites.

5.2. Subthreshold Events 21318591 and 58125945

The cuts associated with the initial unblinding of the searches, which had underestimated the background estimate due to an inadvertent histogram binning mismatch, had events 21318591 and 58125945 as candidates. These events would represent the result of a valid albeit less sensitive search with slightly higher efficiency and a significantly higher (by a factor of 2-3) background estimate. We briefly discuss these events here for completeness and transparency.

Event 21318591 was initially considered a candidate in multiple searches (NGC 1068, SN, Flaring Blazars), although, with $\mathcal{F} = 2.3$ and $-\log_{10} \mathcal{O} = 0.4$, it fails the corrected cuts for all searches. It has a much closer association to NGC 1068 ($\mathcal{D} = 0.64$) and SN ($\mathcal{D} = 0.78$, nearest SN is SN2014dy) than to the blazar search ($\mathcal{D} = 0.955$, nearest blazar is 4C +01.02). The waveform is relatively impulsive, although generally less impulsive than simulated neutrino events, but the polarization—close to equal for HPol and VPol—is atypical for a neutrino event. Moreover, a look at the closest geospatial neighboring events reveals that they have similar waveform shapes and polarization and are moreover also relatively close in time. The anthropogenic isolation cut does not consider how alike or time-correlated neighbors are (although that would be a useful future enhancement), so this additional information may qualitatively suggest an anthropogenic origin.

Event 58125945 was initially identified as very closely associated with TXS 1100+122, with the reconstructed

Details about identified events

	Candidate Ev. 83134914	Subthreshold Ev. 21318591	Subthreshold Ev. 58125945
Time	2015-01-08-19:04:24.237	2014-12-22-04:30:24Z	2015-01-01-08:17:14.615Z
Est. Ice Pos..	98.2E, 68.6S	81.8S, 94.7E	74.4S, 100.3W
Est. Sky Pos.	$\alpha' = 206^\circ, \delta' = 13.6^\circ$	$\alpha' = 38^\circ, \delta' = -3.1^\circ$	$\alpha' = 164^\circ, \delta' = 11.7^\circ$
Potential Associations	SN 2014 D ($\mathcal{D} = 0.67$)	4C +01.02 ($\mathcal{D} = 0.955$) NGC 1068 ($\mathcal{D} = 0.64$) SN 2014dy ($\mathcal{D} = 0.78$)	TXS 1100+122 ($\mathcal{D} = 0.003$)
\mathcal{F}	3.03	2.28	3.06
$-\log_{10} \mathcal{O}$	$\sim \infty$	0.41	0.68

Table 3. Details about the candidate event and subthreshold events that were associated with searches. Event 83134914 was identified by the SN search as potentially associated with SN 2015D. This event was previously identified in the diffuse ANITA-III analysis. The other two events were subthreshold but included here for completeness.

position lying within a degree of the blazar. With $-\log_{10} \mathcal{O} = 0.7$, it (marginally) fails the corrected isolation cut. This event is extremely impulsive and is virtually purely VPol, but appears to point to thin ice within Pine Island Glacier, a part of the continent with relatively low likelihood to produce detectable Askaryan neutrino events. Over the pointing uncertainty of the event, the ice thickness varies from sea ice to 1.2 km. Pine Island Glacier is relatively warm, implying relatively high radio attenuation in its ice. This event is somewhat isolated, but its nearest neighbors, which themselves form a cluster of dozens of events, are similarly impulsive and also mostly VPol. We cannot rule out that this event is a pointing reconstruction outlier from this larger cluster. The British Antarctic Survey was conducting radar and drilling studies in Pine Island Glacier during the 2014-2015 season (Mulvaney & Smith 2017), however due to a powerful storm on January 1, there was no significant activity during the time of the event (Mulvaney 2020). The powerful storm additionally admits the possibility of triboelectric emission (Smith et al. 2020).

Despite these significant caveats, due to the apparent close association with TXS 1100+122, a review of the astrophysical literature on this object is worth presenting. TXS 1100+122 was first observed in gamma-rays (Ojha et al. 2013) in a 2013 flare, followed by the early January 2015 (Pursimo et al. 2015) flare detected by FAVA and therefore entering this object into this analysis. The gamma-ray flare had a hard spectrum and was coincident with an optical flare of two magnitudes. More recently, TXS 1100+122 has been suggested as a potentially interesting neutrino source (Kovalev et al. 2020), on the basis of TXS 1100+122 being compatible in position with IceCube alert event (IC-200109A (IceCube Collaboration 2020)) and possessing a compact ra-

dio emission core, a feature suggested as possibly being associated with neutrino emission (Plavin et al. 2020).

5.3. Limits

As we do not find any significant associations, we proceed to set upper limits on fluence during the ANITA-III flight from each source. Model-independent limits on fluence at a given energy $\Phi(E)$ are given by

$$u.l.(E^2 \Phi(E)) = \left\langle \frac{FC_{90}(n_{obs}, \mu_{bg}) \cdot E}{\epsilon A_{eff}(E) \cdot \Delta} \right\rangle, \quad (5)$$

where Δ is a factor compensating for the use of discrete energies, while the flux and acceptance both evolve continuously. ANITA cosmogenic searches have typically used $\Delta = 4$ (Cremonesi et al. 2019), based on studies showing that this is a reasonable choice for a variety of models (Kravchenko et al. 2006). We maintain this convention here for consistency, but note that other experiments use different conventions.

For objects in source classes with multiple members, setting a limit is slightly more involved. While it is straightforward to calculate the effective area and efficiency given the cuts for each source within the class, partitioning the background estimate is somewhat more complex, as the background estimate was assigned for the entire class, not any particular object. However, assuming zero background for the purpose of setting limits on each source will produce conservative upper limits with small error. The true answer is bounded by ascribing zero background to a source and ascribing the total background of the source class to a source, and this difference is small ($\mathcal{O}(10\%)$) in all cases. Upper limits for each source are shown in Fig. 6. Some sources are omitted due to a paucity of simulated triggered events or low analysis efficiency.

In addition to model-independent energy-dependent limits, we show integrated $\gamma = 2$ limits for AGN-like and

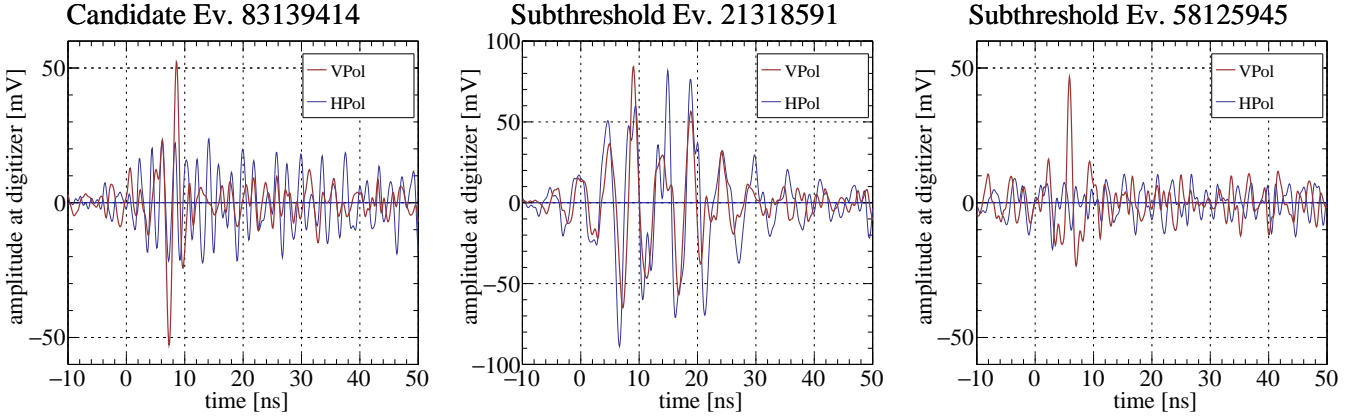


Figure 5. The candidate event (left) and two subthreshold events identified in this analysis. These waveforms represent a coherent sum based on the estimated radio direction and with the group delay from filters and antennas removed.

SN searches, where the upper limit on normalization for a $\Phi(E) = \Phi_0(E^{-2})$ is calculated using:

$$u.l.(\Phi_0) = \left\langle \frac{FC_{90}(n_{obs}, \mu_{bg}) \cdot \phi_0}{\langle \epsilon \cdot A_{eff}(E) \rangle |_{\phi(E)}} \right\rangle, \quad (6)$$

where A_{eff} and ϵ are averages over the unity-normalized flux $\phi(E) = \phi_0 E^{-2}$, with $\phi_0 = 1.00$ EeV for the energy range considered.

The measured fluence for the apparent 2014-2015 TXS 0506+056 neutrino flare from IceCube was $E^2 \Phi(E) = (0.21^{+0.09}_{-0.07}) \text{ GeV cm}^{-2} (E/10^5 \text{ GeV})^{2-2.1 \pm 0.2}$ over a Gaussian window centered on 2014-12-14 ± 14 days with a width of 110^{+34}_{-24} days (Aartsen et al. 2018b). The ANITA-III flight time represents a fraction of 0.16 of this time window. This fluence band, scaled to the ANITA-III flight time, is projected onto the top-left panel of Fig. 6.

6. CONCLUSION AND OUTLOOK

We find that there is no significant evidence for any source-associated neutrinos with ANITA-III, although the potential SN association of the ANITA-III diffuse analysis event is somewhat intriguing, especially in combination with previous results. Given that the analysis efficiency of the ANITA-III diffuse search was quite high, this is perhaps not too surprising a result, as there is relatively little phase space for neutrinos that would trigger ANITA-III but not pass diffuse analysis cuts. As evinced by the subthreshold events identified, further loosening the cuts does lead to additional events, but the higher background limits the discovery potential. Still, using this methodology we are able to set limits on individual sources, which could not be done coherently in the diffuse search. A similar search is in progress for the more recent and more sensitive ANITA-IV payload.

The discovery potential of the methods described here would be improved in cases where there is additional

room between the trigger efficiency and diffuse-search analysis efficiency, suggesting that it is still advantageous to reduce trigger thresholds significantly below the effective analysis threshold for a diffuse search. This could not be achieved in ANITA-III as the acquisition system could not handle the increased data rate from significantly reducing the trigger threshold. Moreover, significant effort in thermal noise reduction and spatial clustering was able to substantially improve the analysis efficiency compared to ANITA-I and ANITA-II. However, a significant gap between analysis and trigger efficiency currently exists in some current in-ice UHE neutrino experiments, such as ARA (Allison et al. 2020), which could benefit from an adaptation of the methods described here. Future UHE neutrino detectors using the Askaryan method such as PUEO (Allison et al. 2020, in preparation), RNO-G (Aguilar et al. 2020, in preparation), or the radio extension of IceCube-Gen2 (Aartsen et al. 2020b) may also benefit from similar methods if the trigger threshold can be made sufficiently low.

ACKNOWLEDGEMENTS

ANITA-III was supported by NASA grant NNX11AC44G, and ANITA-IV was supported by NASA grant NNX15AC24G. We thank the staff of the Columbia Scientific Balloon Facility for their generous support as well as logistical support provided by the National Science Foundation and United States Antarctic Program. This work was supported by the Kavli Institute for Cosmological Physics at the University of Chicago. Computing resources were provided by the Research Computing Center at the University of Chicago and the Ohio Supercomputing Center at The Ohio State University. A. Connolly would like to thank the National Science Foundation for their support through CAREER award 1255557. O. Banerjee and L. Cremonesi's work was supported by collaborative visits

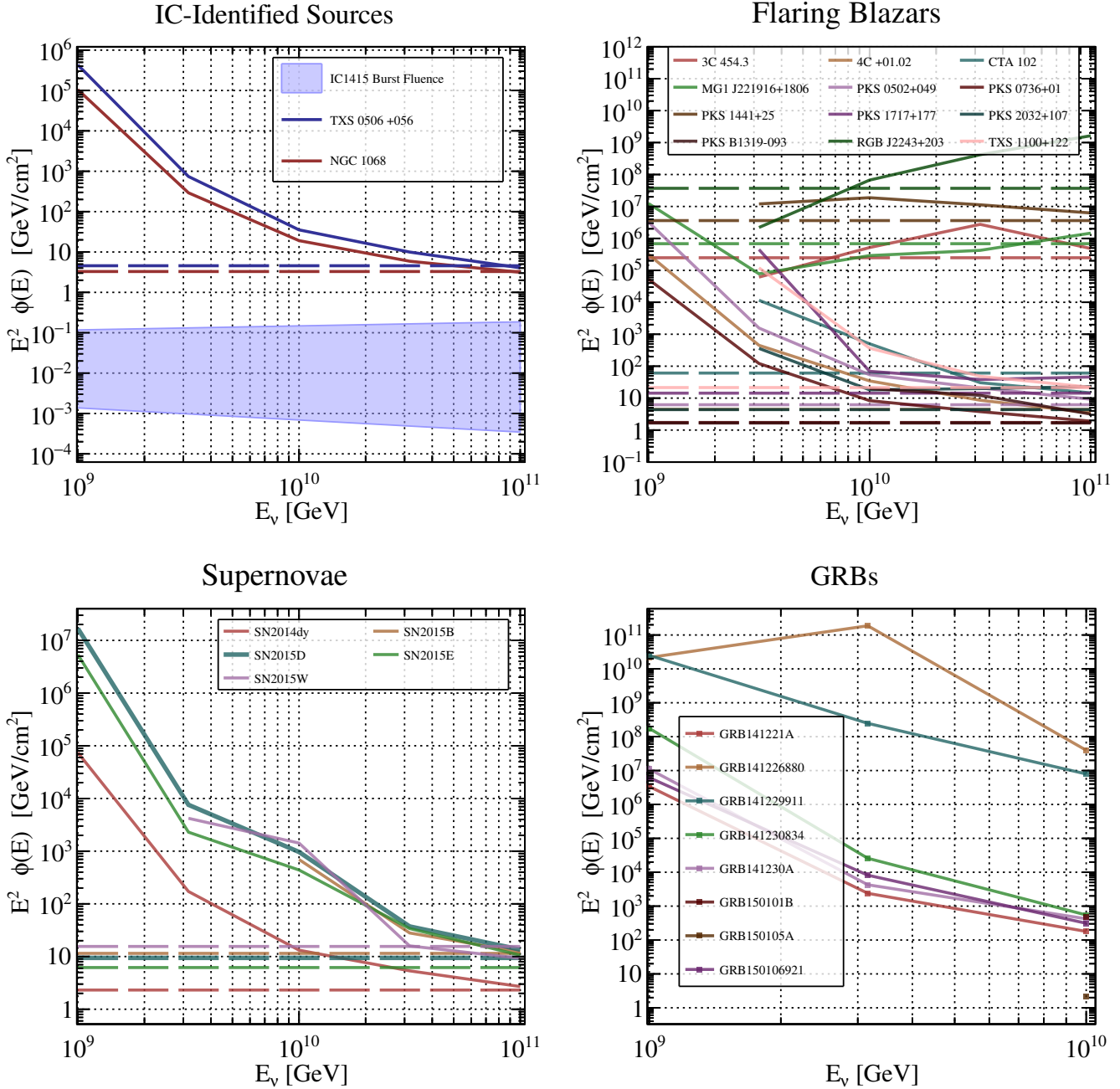


Figure 6. ANITA-III limits on neutrino fluence for all objects considered in these searches. The top-left panel shows fluence limits on TXS 0506+056 and NGC 1068, along with the extrapolated time-scaled fluence from the 2014-2015 apparent IceCube neutrino burst from the direction of TXS 0506+056. The top right shows flaring blazars that result in triggered simulated events (points are not shown when at energies with no simulated passing events). Some blazars (e.g RBG J2243+203) suffer from poor geometry. The bottom left shows SN and the bottom right shows GRBs. Model-independent limits are shown with solid lines and integrated E^{-2} limits are shown with dashed lines, where appropriate.

funded by the Cosmology and Astroparticle Student and Postdoc Exchange Network (CASPER). The University College London group was also supported by the Leverhulme Trust. The National Taiwan University group is supported by Taiwan's Ministry of Science and Technology (MOST) under its Vanguard Program 106-2119-M-002-011. We thank Robert Mulvaney of the

British Antarctic Survey for helpful information about BAS activities around the Pine Island Glacier.

Software: ROOT (Rademakers et al. 2019; Brun & Rademakers 1997), TMVA (Hoecker et al. 2007), icemc (Cremonesi et al. 2019), ANITA Collaboration Software (<https://github.com/anitaNeutrino>, Gorham et al. (2018a))

REFERENCES

Aartsen, M. G., et al. 2013, *Science*, 342, doi: [10.1126/science.1242856](https://doi.org/10.1126/science.1242856)

—. 2018a, *Science*, 361, eaat1378, doi: [10.1126/science.aat1378](https://doi.org/10.1126/science.aat1378)

—. 2018b, *Science*, eaat2890, doi: [10.1126/science.aat2890](https://doi.org/10.1126/science.aat2890)

—. 2020a, *Phys. Rev. Lett.*, 124, 051103, doi: [10.1103/PhysRevLett.124.051103](https://doi.org/10.1103/PhysRevLett.124.051103)

—. 2020b. <https://arxiv.org/abs/2008.04323>

Abdollahi, S., et al. 2017, *Astrophys. J.*, 846, 34, doi: [10.3847/1538-4357/aa8092](https://doi.org/10.3847/1538-4357/aa8092)

Acero, F., et al. 2015, *Astrophys. J. Suppl.*, 218, 23, doi: [10.1088/0067-0049/218/2/23](https://doi.org/10.1088/0067-0049/218/2/23)

Aguilar, J., et al. 2020, in preparation, Design and Sensitivity of the Radio Neutrino Observatory in Greenland (RNO-G)

Allison, P., et al. 2020, *Phys. Rev. D*, 102, 043021, doi: [10.1103/PhysRevD.102.043021](https://doi.org/10.1103/PhysRevD.102.043021)

—. 2020, in preparation, The Payload for Ultrahigh Energy Observations (PUEO): A White Paper

Alves Batista, R., & Silk, J. 2017, *Phys. Rev. D*, 96, 103003, doi: [10.1103/PhysRevD.96.103003](https://doi.org/10.1103/PhysRevD.96.103003)

Askaryan, G. 1962, *Sov. Phys. JETP*, 14 (2), 441

Biehl, D., Boncioli, D., Lunardini, C., & Winter, W. 2018, *Sci. Rep.*, 8, 10828, doi: [10.1038/s41598-018-29022-4](https://doi.org/10.1038/s41598-018-29022-4)

Brun, R., & Rademakers, F. 1997, *Nucl. Instrum. Meth. A*, 389, 81, doi: [10.1016/S0168-9002\(97\)00048-X](https://doi.org/10.1016/S0168-9002(97)00048-X)

CBAT. 2015, CBAT SN catalog

Coppin, P. 2020, GRBWeb. https://icecube.wisc.edu/~grbw_web_public/

Cousins, R. D., & Highland, V. L. 1992, *Nucl. Instrum. Meth. A*, 320, 331, doi: [10.1016/0168-9002\(92\)90794-5](https://doi.org/10.1016/0168-9002(92)90794-5)

Cremonesi, L., et al. 2019, *JINST*, 14, P08011, doi: [10.1088/1748-0221/14/08/P08011](https://doi.org/10.1088/1748-0221/14/08/P08011)

Feldman, G. J., & Cousins, R. D. 1998, *Phys. Rev. D*, 57, 3873, doi: [10.1103/PhysRevD.57.3873](https://doi.org/10.1103/PhysRevD.57.3873)

Fretwell, P., et al. 2013, *Cryosphere*, 7, 375, doi: [10.5194/tc-7-375-2013](https://doi.org/10.5194/tc-7-375-2013)

Gorham, P. W., et al. 2007, *Phys. Rev. Lett.*, 99, 171101, doi: [10.1103/PhysRevLett.99.171101](https://doi.org/10.1103/PhysRevLett.99.171101)

—. 2009a, *Astropart. Phys.*, 32, 10, doi: [10.1016/j.astropartphys.2009.05.003](https://doi.org/10.1016/j.astropartphys.2009.05.003)

—. 2009b, *Phys. Rev. Lett.*, 103, 051103, doi: [10.1103/PhysRevLett.103.051103](https://doi.org/10.1103/PhysRevLett.103.051103)

—. 2010, *Phys. Rev. D*, 82, 022004, doi: [10.1103/PhysRevD.82.022004](https://doi.org/10.1103/PhysRevD.82.022004)

—. 2018a, *Phys. Rev. D*, 98, 022001, doi: [10.1103/PhysRevD.98.022001](https://doi.org/10.1103/PhysRevD.98.022001)

—. 2018b, *Phys. Rev. Lett.*, 121, 161102, doi: [10.1103/PhysRevLett.121.161102](https://doi.org/10.1103/PhysRevLett.121.161102)

—. 2019, *Phys. Rev. D*, 99, 122001, doi: [10.1103/PhysRevD.99.122001](https://doi.org/10.1103/PhysRevD.99.122001)

Greisen, K. 1966, *Phys. Rev. Lett.*, 16, 748, doi: [10.1103/PhysRevLett.16.748](https://doi.org/10.1103/PhysRevLett.16.748)

Hoecker, A., et al. 2007, PoS, ACAT2007, 040

IceCube Collaboration. 2020, GRB Coordinates Network, 26696, 1

Jin, Z. w., et al. 2015, *Central Bureau Electronic Telegrams*, 4051, 1

Kotera, K., Allard, D., & Olinto, A. V. 2010, *J. Cosmol. Astropart. Phys.*, 10, 13, doi: [10.1088/1475-7516/2010/10/013](https://doi.org/10.1088/1475-7516/2010/10/013)

Kovalev, Y. Y., et al. 2020, *The Astronomer's Telegram*, 13397, 1

Kravchenko, I., et al. 2006, *Phys. Rev. D*, 73, 082002, doi: [10.1103/PhysRevD.73.082002](https://doi.org/10.1103/PhysRevD.73.082002)

Li, T. P., & Ma, Y. Q. 1983, *ApJ*, 272, 317, doi: [10.1086/161295](https://doi.org/10.1086/161295)

Lien, A., et al. 2016, *Astrophys. J.*, 829, 7, doi: [10.3847/0004-637X/829/1/7](https://doi.org/10.3847/0004-637X/829/1/7)

Mulvaney, R. 2020, Private Communication

Mulvaney, R., & Smith, A. M. 2017, NERC Polar Data Centre, doi: [10.5285/ea547d0-9668-4ba1-9fc4-67929382395f](https://doi.org/10.5285/ea547d0-9668-4ba1-9fc4-67929382395f)

Ojha, R., Carpenter, B., & Cheung, C. C. 2013, *The Astronomer's Telegram*, 5202, 1

Plavin, A., Kovalev, Y., Kovalev, Y., & Troitsky, S. 2020, *Astrophys. J.*, 894, 101, doi: [10.3847/1538-4357/ab86bd](https://doi.org/10.3847/1538-4357/ab86bd)

Pursimo, T., Ojha, R., & Kocevski, D. 2015, *The Astronomer's Telegram*, 6914, 1

Rademakers, F., et al. 2019, root-project/root: v6.18/02, v6-18-02, Zenodo, doi: [10.5281/zenodo.3895860](https://doi.org/10.5281/zenodo.3895860).
<https://doi.org/10.5281/zenodo.3895860>

Righi, C., et al. 2020. <https://arxiv.org/abs/2003.08701>

Rodrigues, X., et al. 2020.
<https://arxiv.org/abs/2003.08392>

Smith, D., et al. 2020. <https://arxiv.org/abs/2009.13010>

Vieregg, A., et al. 2011, *Astrophys. J.*, 736, 50,
doi: [10.1088/0004-637X/736/1/50](https://doi.org/10.1088/0004-637X/736/1/50)

von Kienlin, A., Meegan, C. A., Paciesas, W. S., et al. 2020, *The Astrophysical Journal*, 893, 46,
doi: [10.3847/1538-4357/ab7a18](https://doi.org/10.3847/1538-4357/ab7a18)

Wang, X.-Y., Razzaque, S., Meszaros, P., & Dai, Z.-G. 2007, *Phys. Rev. D*, 76, 083009,
doi: [10.1103/PhysRevD.76.083009](https://doi.org/10.1103/PhysRevD.76.083009)

Waxman, E., & Bahcall, J. N. 2000, *Astrophys. J.*, 541, 707, doi: [10.1086/309462](https://doi.org/10.1086/309462)

Zatsepin, G., & Kuzmin, V. 1966, *JETP Lett.*, 4, 78